ACS APPLIED ENERGY MATERIALS

www.acsaem.org Article

Boosting the Low-Temperature Performance of Graphite Anodes by Creating an Electrochemically Active Interface

Yikang Yu, Mitchell I. Levine, Zhenzhen Yang, Sungho Jeon, Eric A. Stach, and Jian Xie*

Cite This: ACS Appl. Energy Mater. 2023, 6, 12371−12378 Read Online

ACCESS | Metrics & More | Article Recommendations | Supporting Information

Downloaded via UNIV OF PENNSYLVANIA on March 19, 2024 at 16:02:52 (UTC).
See https://pubs.acs.org/sharingguidelines for options on how to legitimately share published articles.

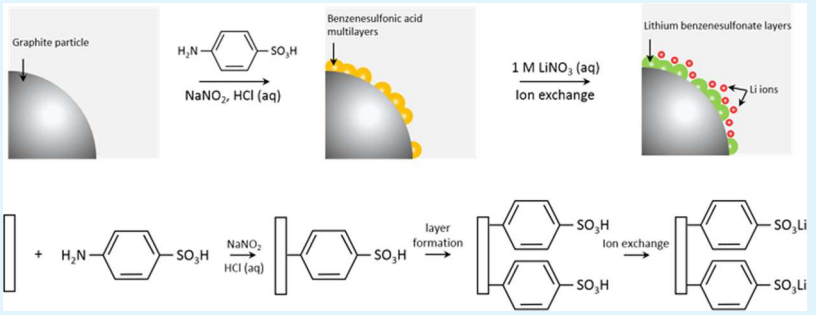

ABSTRACT: Graphite is the major anode material used in commercial lithium-ion batteries (LIBs). However, the sluggish ion-transfer kinetics associated with graphite anodes significantly restrict the operation of LIBs over a wide temperature. This is primarily due to their low reversible capacity and the substantial overpotential exhibited under low-temperature conditions. To address this limitation, we demonstrate herein an approach that involves grafting an electrochemically active lithium benzenesulfonate layer onto a graphite surface through a typical reduction reaction of diazonium cations, followed by ion exchange process. This surface modification reduces the charge transfer resistance of graphite anodes, leading to an excellent reversible capacity of ∼150 mAh g^{-1} at low-temperatures (−20 °C, 0.1C). Electrochemical impedance spectroscopy indicates that both desolvation of the lithium ions outside the graphite, and lithium diffusion within the solid electrolyte interphase and graphite lattice are two crucial rate-limiting steps during the Li (de)lithiation, with the latter dominating during the low-temperature operation. These findings demonstrate a facile method for enhancing the low-temperature performance of graphite through surface modification and provide valuable insights into fundamental understandings that can guide the future design of better -low-temperature graphite anodes.

KEYWORDS: *lithium-ion batteries, graphite anodes, low-temperature performance, surface modifications, lithium diffusion*

1. INTRODUCTION

Despite significant advancements in high-capacity anode materials over the past decades,[1−3] graphite remains the predominant choice as the anode material used in lithium-ion batteries due to its abundance, low cost, and long cycle life.[4−7] However, conventional graphite materials have sluggish intercalation kinetics, leading to metallic lithium plating and low specific capacity during high-rate operation.[8−11] These limitations are exacerbated when the graphite is used at low-temperatures (e.g., − 10 °C), resulting in significantly reduced reversible capacity and increased overpotential.[12−14] The inadequate performance of graphite anodes at subzero temperatures significantly hinders the widespread adoption of electric vehicles in cold-weather regions worldwide.

Typically, the major rate-limiting processes during low-temperature operations are considered to be the diffusion of lithium ions within the host materials and the desolvation of solvated Li ions occurring at the electrode and electrolyte surface.[15−18] Based on this understanding, there are many efforts have been paid to modify the surface of graphite and manipulate the solid electrolyte interphase (SEI) to facilitate the Li-ion diffusion into the graphite surface.[19−22] However, it has proven to be challenging to tailor the structure of the SEI so that it allows fast charge transfer. This is because the SEI is composed of a complex combination of organic and inorganic components, formed by preferential reduction of the electrolyte.[1,23,24] Apart from the SEI design which is based on electrolyte additives, the tuning of interaction between the solvents and the Li ions in the electrolyte has received increasing attention in recent years.[14,25] The weak interaction between the solvents and Li ions is able to reduce the charge transfer resistance and, thus, improve the low-temperature performance. In contrast, the direct modification of graphite

Received: August 30, 2023
Revised: November 28, 2023
Accepted: November 29, 2023
Published: December 14, 2023

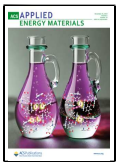

© 2023 American Chemical Society

https://doi.org/10.1021/acsaem.3c02203
ACS Appl. Energy Mater. 2023, 6, 12371−12378

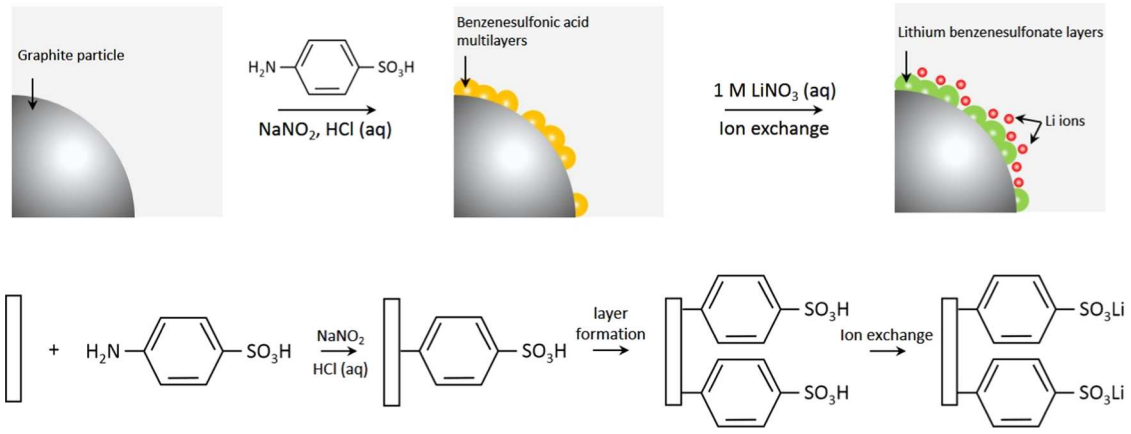

Figure 1. Illustration of the formation process of the lithium benzenesulfonate layer (LBL) on the graphite surface.

via surface etching has shown the potential to increase Li-ion intercalation sites and thus enhance lithium intercalation kinetics.[26] Additionally, surface coatings, such as specific carbon structures and Al_2O_3, have been reported to enhance the rate performance of graphite by promoting rapid lithium surface diffusion and improving wetting between graphite and electrolyte.[10,27,28] However, the electrochemical activity of those coating layers, especially the Li diffusion behavior across those layers, remains unclear.

As noted above, Li-ion diffusion through the SEI is significantly suppressed with the reduced temperature, and the low-temperature performance of graphite is controlled by diffusion to a large extent. Lithium benzenesulfonate has been reported as a material capable of enhancing lithium diffusion due to its electrochemically active nature.[29] In this study, graphite anodes grafted with a lithium benzenesulfonate layer (LBL-modified graphite) are prepared, using a typical reduction reaction of diazonium cation.[30] The subsequent ion exchange introduces a distribution of Li ions on the surface of the LBL-modified graphite. This electrochemically active layer facilitates lithium diffusion across the graphite surface, promoting charge transfer during low-temperature operation. The formation of the lithium benzenesulfonate layer was confirmed through scanning electron microscopy (SEM) coupled to X-ray photoelectron spectroscopy (XPS). The presence of this "artificial SEI" led to an increase in the initial Coulombic efficiency from 77.4% (pristine graphite) to 85.9%, suggesting a suppressed SEI formation. The cycling performance and capacity retention at a low-temperature (−20 °C) were further examined and compared with those of the pristine graphite anodes. To gain a deeper understanding of the intercalation kinetics and charge transfer limitations during low-temperature operation, electrochemical impedance spectroscopy (EIS) was employed to analyze performance limitations.[31] It was observed that the lithium benzenesulfonate layer on the graphite surface greatly reduced charge transfer resistance, resulting in an improved low-temperature capacity retention (0.1C, ∼150 mAh g^{-1}) of 44.8% compared with that of pristine graphite (∼122 mAh g^{-1}, 37.0%).

2. METHODS

2.1. Materials. Graphite powders (MescoCarbon MicroBeads, MCMB), Li foil (15.8 mm), and Super P conductive carbon were purchased from MTI Corporation. Battery grade $LiPF_6$, ethyl methyl carbonate (EMC), ethylene carbonate, and lithium bis-(trifluoromethanesulfonyl)imide (LiTFSI) were supplied by Novolyte Technologies. Fluoroethylene carbonate (98.0%, FEC) and ethyl trifluoroacetate (99.0%, ETFA) were obtained from TCI and Thermo Scientific Chemicals, respectively. Sulfanilic acid (98.0%) and sodium nitrite (99.0%, $NaNO_2$) were purchased from Alfa Aesar.

2.2. LBL-Modified Graphite Preparation. The LBL-modified graphite was prepared based on a reduction reaction of diazonium cation, well known for electrochemical derivatization of carbon surfaces.[32,33,30] First, 1 g of graphite powder was dispersed in 300 mL of a 1 M HCl solution with the addition of 0.02 mol of sulfanilic acid. The solution was vigorously stirred for 30 min before sodium nitrite addition. 0.04 mol of $NaNO_2$ was then introduced, and the mixture was stirred for another 3 h at 70 °C. The final product was then filtered, washed with water, and dispersed in 100 mL of 1 M $LiNO_3$ aqueous solution for ion exchange, accomplished by stirring overnight. The LBL-modified graphite was obtained by filtration, washing with water, and oven-drying, successively.

2.3. Electrode Preparation. The electrode used in the coin cells was prepared by slurry coating on a Cu foil, composed of 80 wt % graphite (or LBL-modified graphite), 10 wt % Super P, and 10 wt % poly(vinylidene difluoride) (PVDF). The mass loading of the electrode is about 1.5 mg cm^{-2}.

2.4. Electrochemical and Materials Characterization. The electrochemical tests were conducted based on a CR2032-type coin cell. Typically, a Li foil was used as the counter/reference electrode, and as-prepared electrodes (graphite or LBL-modified graphite) were used as the working electrodes with one piece of polypropylene separator (Celgard 2400). 50 μL of EC-based (1.2 M $LiPF_6$ in EC−EMC, 3:7 by mass) or FEC-based (1 M LiTFSI in FEC−ETFA, 3:7 by mass) electrolyte was used in each cell for room-temperature or low-temperature (−20 °C) operation. The cutoff voltage was controlled at 0.005−2.0 V (vs Li^+/Li). The galvanostatic charge and discharge were collected on a LAND-CT2001 battery testing instrument at a determined C rate (1C = 372 mA g^{-1}). The electrochemical impedance spectroscopy (EIS) was measured by a Solartron potentiostat with an AC voltage of 10 mV in the frequency range from 600 kHz to 0.1 Hz (model SI 1287). The pristine graphite and LBL-modified graphite electrodes were examined using the X-ray powder diffraction technique (Cu Kα, Bruker D8 Discover) to investigate their crystal structure. Scanning electron microscopy (SEM) images and corresponding energy-dispersive spectrometry (EDS) images were acquired from JEOL 7800F field emission SEM facilities with an operation voltage of 5 kV. Scanning transmission electron microscopy (STEM) images and related EDS and EELS data (elemental mapping and spectra) were obtained by using a JEOL NEOARM instrument operated at 200 kV. For imaging, the camera length used with the JEOL NEOARM was 4 cm, with a probe current of 500 pA. For EDS and EELS, the camera length was 2 cm, and the probe current was 700 pA. X-ray photoelectron spectroscopy (XPS) data was acquired using a PHI 5000 VersaProbe II system.

https://doi.org/10.1021/acsaem.3c02203
ACS Appl. Energy Mater. 2023, 6, 12371−12378

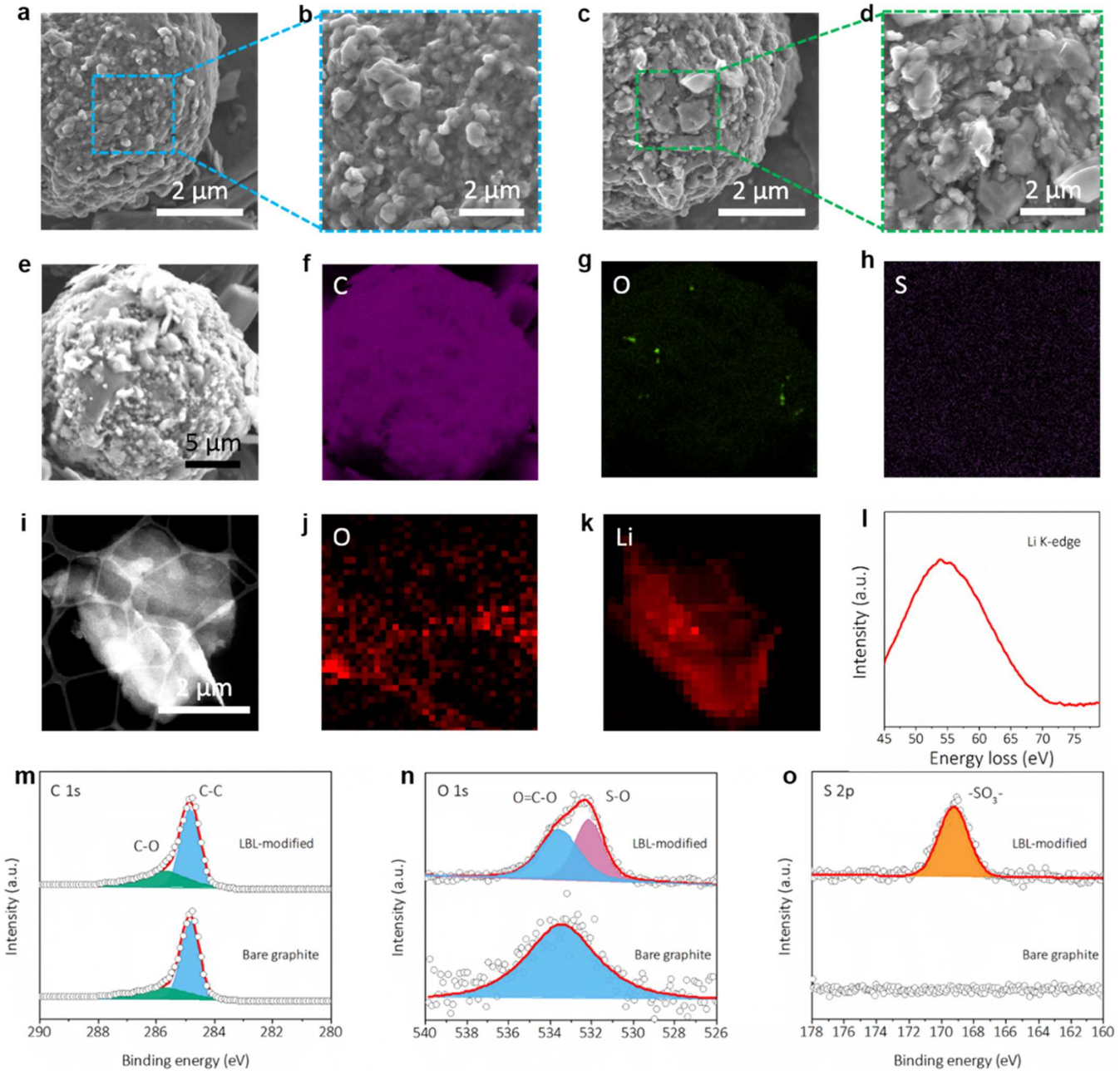

Figure 2. Morphologies and components of the electrochemically active interface on the graphite surface. SEM image of pristine graphite (a, b) and LBL-modified graphite (c, d). SEM images of an LBL-modified graphite particle (e) with corresponding EDS mapping images with carbon (f), oxygen (g), and sulfur (h). STEM image of LBL-modified graphite (i) with corresponding EDS and EELS maps of oxygen (j) and lithium (k) signals, respectively. (l) Characteristic Li K-edge EELS. XPS spectra of pristine graphite and LBL-modified graphite with C 1s spectra (m), O 1s spectra (n), and S 2p spectra (o).

3. RESULTS AND DISCUSSION

The grafting of aryl diazonium salts onto the graphite surface has been previously explored as an effective means to enhance electrochemical performance.[34−37] These layers can act as a stable and compact artificial solid electrolyte interphase (SEI), providing protection to graphite particles during (de)lithiation. However, to the best of our knowledge, these layers have rarely been designed as electrochemically active layers to facilitate lithium diffusion on the graphite surface. Inspired by the recent findings regarding the electrochemically active nature of the lithium benzenesulfonate layer for enhancing lithium diffusion,[29] we have designed a similar layer to be grafted onto the graphite surface directly. This process is accomplished through a typical reduction reaction of diazonium cation,[30] as depicted in Figure 1. After ion exchange, in which protons are replaced with Li ions, graphite with the lithium benzenesulfonate layer (LBL-modified graphite) was successfully obtained after subsequent washing and drying.

The surface structure and chemical composition of LBL-modified graphite were investigated using a combination of electron microscopy and X-ray photoelectron spectroscopy (XPS). Scanning electron microscopy (SEM) images show a complete LBL-modified particle (Figure 2c) similar to pristine graphite (Figure 2a), indicating that the surface reaction occurs without damaging the graphite particle during the reduction

https://doi.org/10.1021/acsaem.3c02203
ACS Appl. Energy Mater. 2023, 6, 12371−12378

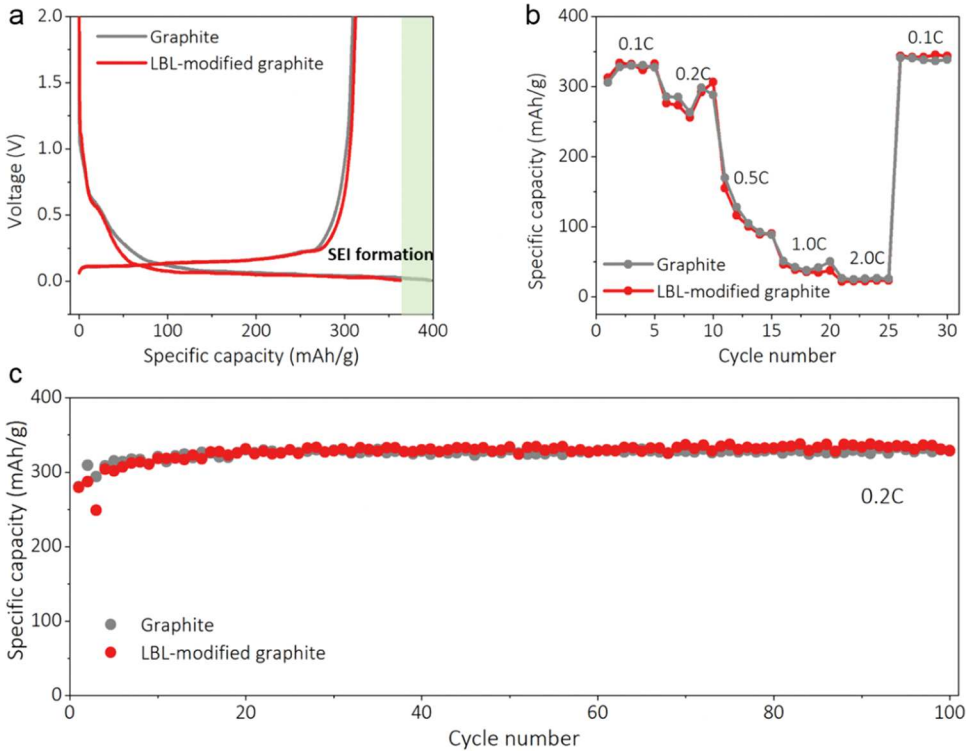

Figure 3. Electrochemical performance under room-temperature conditions. (a) Initial charge and discharge curves of graphite and the LBL-modified graphite at 0.1C, in which an increased ICE is demonstrated by the LBL-modified graphite due to the suppressed SEI formation. C-rate (b) and longtime cycling (c) performance of graphite and LBL-modified graphite.

reaction of diazonium cation and ion exchange. Moreover, X-ray diffraction (XRD) patterns (Figure S1) show a typical graphite structure with two characteristic peaks without any noticeable shift compared with pristine graphite, which further validates that graphite crystal structure is not destroyed during the preparation process of LBL-modified graphite. Higher-magnification SEM images also show a limited surface difference on the LBL-modified graphite (Figure 2d) compared with pristine graphite (Figure 2b). Moreover, the corresponding SEM energy-dispersive X-ray spectroscopy maps were acquired to understand the elemental distribution on the LBL-modified graphite surface (Figure 2e–h). In addition to the strong carbon signals (Figure 2f), a clear oxygen signal corresponding to the grafting of the $-SO_3Li$ group on the graphite surface is observed. However, a weak sulfur signal is detected from the SEM EDS, making it challenging to determine the sulfur elemental distribution (Figure 2h). To further confirm the success of the ion exchange process, STEM EDS and electron energy loss spectroscopy (EELS) elemental mappings were performed (Figure 2i–l). In addition to the oxygen distribution revealed by STEM EDS maps (Figure 2j), a uniform distribution of lithium elements on the LBL-modified graphite surface is further identified by STEM-EELS (Figure 2k). The presence of the lithium element was further confirmed by the EELS spectra, which exhibit the characteristic K-shell ionization edge of lithium at ~55 eV (Figure 2l).[38] To investigate the chemical compositions of the grafted surface layer, XPS measurements were conducted on the LBL-modified graphite and pristine graphite samples. The C 1s spectra show strong C–C bonding (~284.8 eV) along with C–O bonding (~286 eV) for both samples (Figure 2m). In Figure 2n, an evident peak shift from ~534 to ~532 eV is observed in the O 1s spectra after LBL grafting, corresponding to the O=C–O and S–O groups, respectively.[39,40] In particular, a distinct characteristic peak located at ~169 eV in the S 2p spectra represents the $-SO_3-$ group present in LBL-modified graphite (Figure 2o). The combination of information obtained from electron microscopy and XPS confirms the successful grafting of the lithium benzenesulfonate layer onto graphite in our LBL-modified graphite sample.

The electrochemical performance of an LBL-modified graphite compared with pristine graphite at room-temperature is shown in Figure 3. It is evident that the C-rate performance ranging from 0.1C to 2.0C and the cycling stability (0.2C, 150 cycles) of LBL-modified almost remain unchanged after surface layer grafting (Figure 3b,c). Both samples demonstrate a specific capacity of ~330 mAh g^{-1} during low-rate operation (e.g., 0.1C), while a poor capacity of around 25 mAh g^{-1} is observed under high-rate conditions (2.0C). These results indicate that the improvement in Li surface diffusion has a limited impact on the high-rate performance, as the rate-limiting step is governed by the Li diffusion across SEI and solid diffusion of lithium ions within the graphite lattice.[41] However, it is worth noting that the formation of lithium benzenesulfonate layer on the graphite surface significantly suppresses SEI formation, as evident from the enhanced initial Coulombic efficiency (ICE), with ICE increasing from 77.4% for pristine graphite to 85.9% for the LBL-modified graphite (Figure 3a). The increase in ICE helps alleviate the initial lithium loss caused by SEI formation on the graphite anode, thus offsetting the energy density reduction in lithium-ion batteries after the initial charge process.[6,42] Therefore, grafting the surface layer also provides an effective approach to mitigate the initial lithium loss on graphite and increase the energy density of lithium-ion batteries.

https://doi.org/10.1021/acsaem.3c02203
ACS Appl. Energy Mater. 2023, 6, 12371–12378

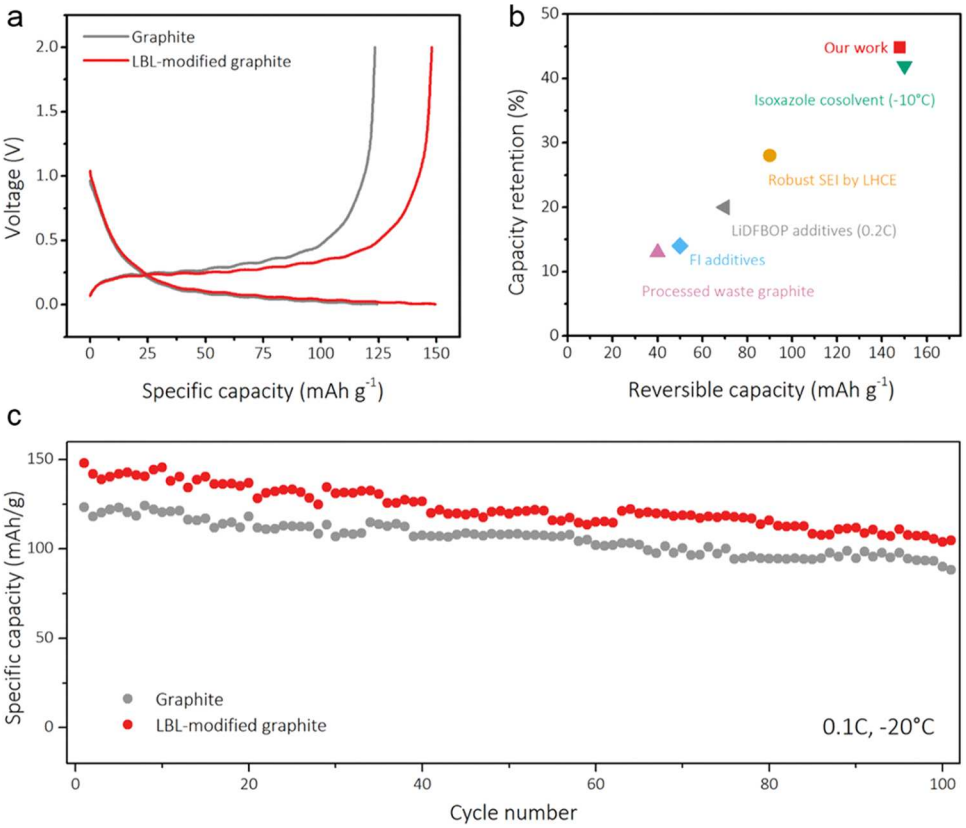

Figure 4. Electrochemical performance during a low-temperature operation (−20 °C). (a) initial charge and discharge curves of pristine graphite and LBL-modified graphite at −20 °C (0.1C). (b) Performance comparison of graphite anode by surface modifications from previous reports with our LBL-modified graphite. The capacity retention shows the low-temperature (−20 °C and 0.1C if not indicated otherwise in the figure) reversible capacity retention percentage compared with room temperature. (c) longtime cycling performance of the LBL-modified graphite and pristine graphite at low temperatures (0.1C).

To evaluate the specific capacity retention and cycling performance of LBL under low-temperature conditions, galvanostatic discharge−charge tests were performed for the LBL-modified graphite and the pristine graphite anode in a low-temperature chamber (−20 °C). Figure 4a exhibits the initial charge and discharge curves of the LBL-modified graphite and graphite at 0.1C. It is evident that the LBL-modified graphite exhibits an improved reversible capacity of ∼150 mAh g^{-1} (Figure 4a) at −20 °C compared with the pristine graphite anode (∼123 mAh g^{-1}), resulting in a capacity retention of ∼45% relative to room-temperature operation (Figure 3a,b). Moreover, voltage hysteresis was calculated based on the difference between the average discharge and charge voltage. It has been found that the LBL-modified graphite shows a slightly lower voltage hysteresis (∼0.22 V) compared with the pristine graphite anode (∼0.23 V), indicating an improved kinetics at low-temperatures. Figure 4b presents the capacity retention and reversible capacity for recent advances in graphite surface modification, including our LBL-modified graphite during low-temperature operation (0.1C and −20 °C if not indicated otherwise in the figure). In comparison to SEI structures improved by electrolyte modification,[12,19−21,43] our LBL-modified graphite demonstrates superior performance with higher reversible capacity and capacity retention for low-temperature conditions (Figure 4b). Furthermore, the longtime cycling of LBL-modified graphite shows a capacity retention of ∼70.7% after 100 cycles at −20 °C (0.1C), which is competitive with those SEI-modified graphite anodes.[21]

To elucidate the rate-limiting steps of the graphite anode operation under low-temperatures, electrochemical impedance spectroscopy (EIS) measurements were conducted using a fitting method based on a previous report.[31] The total impedance was divided into four components: the electrolyte and electrode resistance (R_{ee}), contact resistance (R_{con}), charge transfer resistance (R_{ct}), and diffusion resistance (R_{diff}). The resistance between the electrolyte and electrode reflects the degree of wetting between the electrolyte and electrode, which can be determined by the high-frequency resistance of the cell.[44] The high-frequency semicircle in a typical EIS curve corresponds to the contact resistance between the graphite electrode and the current collector. Furthermore, the subsequent semicircle at high−medium frequency represents the charge transfer resistance (R_{ct}). Typically, diffusion limitations in the electrolyte have much less influence than the lithium diffusion within the graphite, regardless of whether at room-temperature or low-temperature (≥−20 °C). Thus, based on this analysis, the quantification of each individual resistance was performed using the equivalent circuit shown in Figure 5a (inset). After quantifying individual resistances, it was observed that the charge transfer and Li diffusion resistance in the graphite and via diffusion through the SEI were the predominant rate-limiting steps, accounting for over 90% of the resistance contribution in these two processes for both graphite and LBL-modified graphite anodes (Figure 5c).

https://doi.org/10.1021/acsaem.3c02203
ACS Appl. Energy Mater. 2023, 6, 12371−12378

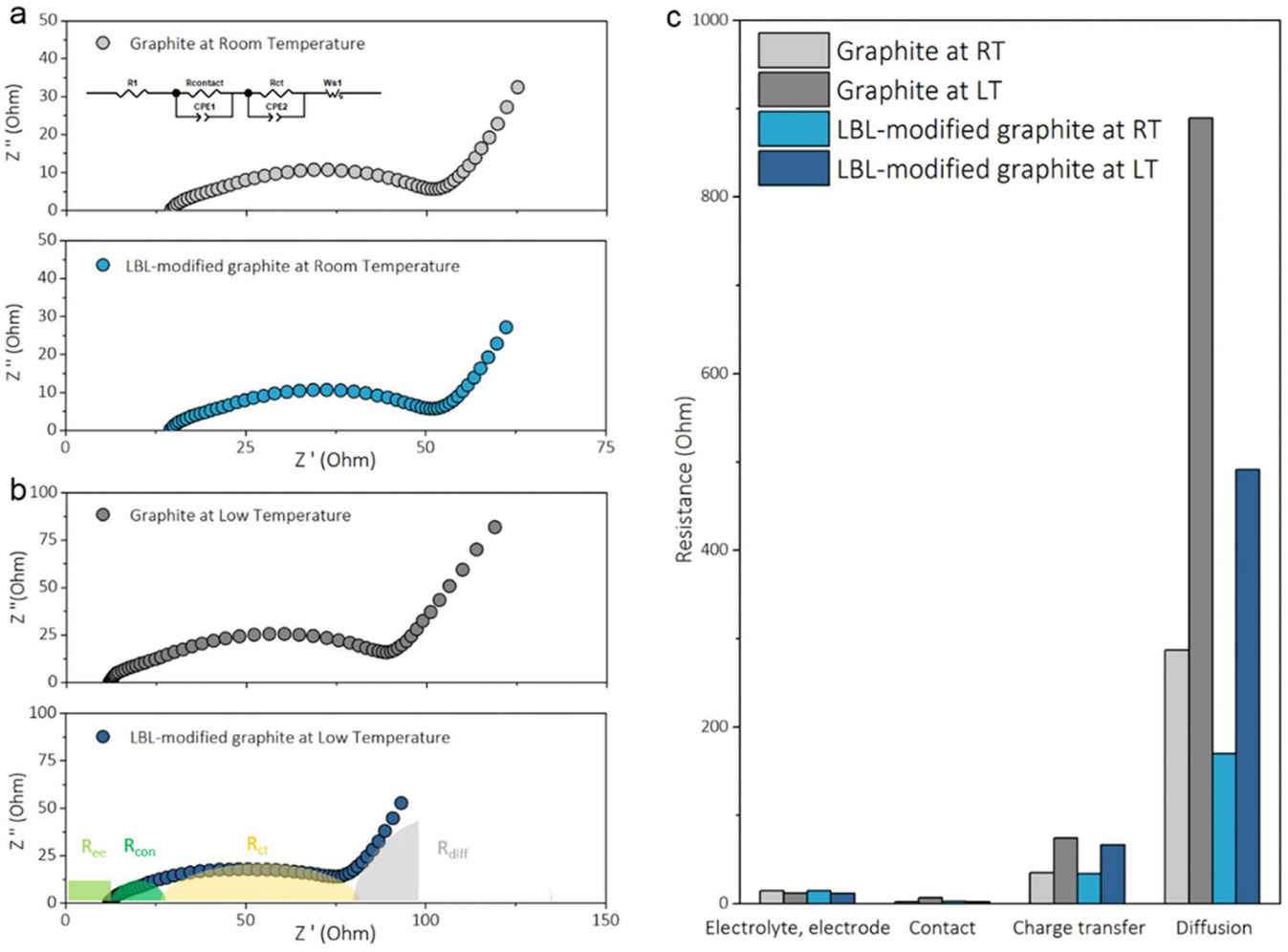

Figure 5. EIS curves for graphite and LBL-modified graphite at room temperature (a) and low temperature (b) with relative contributions (c) of the different steps based on the impedance fitting.

At room temperature, the grafting of the electrochemically active layer with lithium concentration in the LBL-modified graphite negligibly reduced the charge transfer resistance (R_{ct}, ~34.3 Ω) compared with that of pristine graphite (~35.0 Ω, Figure 5a). Conversely, the rate-limiting step should be the lithium-ion diffusion in the graphite lattice and via diffusion through the SEI. In contrast, at low-temperatures, the LBL-modified graphite also exhibited a slight reduction in charge transfer resistance from ~74.3 to ~66.7 Ω in the EIS curve. In general, the charge transfer process of the Li-ion intercalation includes the desolvation of the solvated Li ions in the electrolyte, the Li-ion transport in the solid electrolyte interphase (SEI) layer, and the final acceptance of electrons in the graphite lattice.[18,45,46] However, the real charge transfer process in the graphite anode actually occurs within the graphite bulk and does not involve the diffusion of chemical species in the SEI, while the R_{ct} in the model was associated with the Li-ion solvation sheath.[47] This explains why similar R_{ct} values were observed in both pristine graphite and LBL-modified anodes, independent of temperature since the same electrolyte was used with the same Li-ion solvation sheath. In contrast, the diffusion process consists of Li diffusion in the SEI and graphite lattice. The surface functionalization of lithium-containing groups effectively promotes Li diffusion through the SEI, leading to a greatly suppressed R_{diff} for LBL-modified graphite anode (Figure 5c). To demonstrate the improved surface diffusion further clearly on LBL-modified graphite, a high-temperature cycling test (50 °C and 0.2C) was conducted. At high-temperature operation conditions, the influence of Li diffusion in the graphite lattice and desolvation of the solvated Li ions decreases, which makes the contribution of Li surface diffusion more significant. As expected, the LBL-modified graphite shows a steady specific capacity of ~360 mAh g^{-1} while the pristine graphite anode demonstrates a lower capacity at the initial cycle (227 mAh g^{-1}) and stabilizes to ~320 mAh g^{-1} (Figure S2, 0.2C) at high temperature. The difference in performance at high-temperatures is much more visible compared with that at room-temperature (Figure 3c). Moreover, such a performance further indicates that this lithium benzenesulfonate layer is compatible with a high-temperature operation as high as 50 °C. This results in an improved low-temperature performance. Finally, the large R_{diff} value of LBL-modified graphite and R_{ct} further suggest that the Li diffusion within the graphite lattice and the desolvation of solvated Li ions are the rate-limiting steps for low-temperature operation of graphite anodes.

4. CONCLUSIONS

Graphite with an electrochemically active lithium benzenesulfonate layer was fabricated to facilitate its charge transfer capabilities and improve its performance at low temperatures.

https://doi.org/10.1021/acsaem.3c02203
ACS Appl. Energy Mater. 2023, 6, 12371−12378

The presence of this layer resulted in a suppressed SEI formation, leading to an elevated ICE of 85.9% compared with that of pristine graphite (77.4%). This demonstrates the feasibility of using LBL to compensate for the initial lithium loss in lithium-ion batteries. Moreover, a comprehensive investigation of the low-temperature performance was conducted. The improved reversible capacity and capacity retention of LBL-modified graphite can be attributed to reduced Li diffusion resistances compared with pristine graphite. However, the resistance contributions obtained from fitting the electrochemical impedance spectroscopy (EIS) curves indicate that diffusion within the graphite lattice and desolvation of solvated Li ions remain the major rate-limiting step under low-temperature conditions. Therefore, our findings provide valuable insights for the future design of graphite anodes with a focus on enhancing lithium diffusion kinetics to achieve superior performance at low-temperatures.

■ ASSOCIATED CONTENT

Supporting Information

The Supporting Information is available free of charge at https://pubs.acs.org/doi/10.1021/acsaem.3c02203.

XRD patterns, high-temperature electrochemical performance (PDF)

■ AUTHOR INFORMATION

Corresponding Author

Jian Xie − *Department of Mechanical and Energy Engineering, Purdue School of Engineering and Technology, Indiana University—Purdue University Indianapolis, Indianapolis, Indiana 46202, United States;* orcid.org/0000-0002-9800-0206; Email: jianxie@iupui.edu

Authors

Yikang Yu − *Department of Mechanical and Energy Engineering, Purdue School of Engineering and Technology, Indiana University—Purdue University Indianapolis, Indianapolis, Indiana 46202, United States; School of Mechanical Engineering, Purdue University, West Lafayette, Indiana 47907, United States;* orcid.org/0000-0002-6101-2393

Mitchell I. Levine − *Department of Mechanical and Energy Engineering, Purdue School of Engineering and Technology, Indiana University—Purdue University Indianapolis, Indianapolis, Indiana 46202, United States*

Zhenzhen Yang − *Chemical Sciences and Engineering Division, Argonne National Laboratory, Lemont, Illinois 60439, United States;* orcid.org/0000-0002-1073-3799

Sungho Jeon − *Department of Materials Science and Engineering, University of Pennsylvania, Philadelphia, Pennsylvania 19102, United States*

Eric A. Stach − *Department of Materials Science and Engineering, University of Pennsylvania, Philadelphia, Pennsylvania 19102, United States;* orcid.org/0000-0002-3366-2153

Complete contact information is available at: https://pubs.acs.org/10.1021/acsaem.3c02203

Author Contributions

Y.Y.: Conceived the idea, prepared the materials, and conducted electrochemical tests. M.I.L.: Prepared coin cells and conducted partial electrochemical tests. Z.Y.: Performed the XPS measurements. S.J.: Performed the TEM characterization and analyzed the results. E.A.S.: Supervised the TEM characterization and results. J.X.: Conceived the idea and supervised this project. All authors discussed the results and participated in the manuscript preparation.

Notes

The authors declare no competing financial interest.

■ ACKNOWLEDGMENTS

The authors appreciate Alexander Nickol from Fraunhofer IKTS for the constructive discussion on the EIS curve fitting. This project was partially supported by the Office of Vice Chancellor for Research, Indiana University Purdue University Indianapolis (IUPUI). The authors gratefully acknowledge the help from Post Test Facility at Argonne National Laboratory, supported by the U.S. DOE Vehicle Technologies office, and the use of the Center for Nanoscale Materials, a U.S. Department of Energy Office of Science User Facility, as supported by the U.S. DOE, Office of Basic Energy Sciences, both under contract number DE-AC02-06CH11357. STEM experiments were performed at the Singh Center for Nanotechnology at the University of Pennsylvania, supported by the National Science Foundation (NSF) National Nanotechnology Coordinated Infrastructure Program grant NNCI-1542153. Additional support to the Nanoscale Characterization Facility at the Singh Center has been provided by the Laboratory for Research on the Structure of Matter (MRSEC) supported by the National Science Foundation (DMR-1720530).

■ REFERENCES

(1) Yu, Y.; Liu, Y.; Xie, J. Building Better Li Metal Anodes in Liquid Electrolyte: Challenges and Progress. *ACS Appl. Mater. Interfaces* **2021**, *13* (1), 18−33.

(2) Zuo, X.; Zhu, J.; Müller-Buschbaum, P.; Cheng, Y.-J. Silicon based lithium-ion battery anodes: A chronicle perspective review. *Nano Energy* **2017**, *31*, 113−143.

(3) Zhao, J.; Li, C.-L.; Chen, G.; Ji, F.; Shen, Y.-Y.; Peng, J.; Wang, W.-H. Rational design of Sn4P3/Ti3C2T x composite anode with enhanced performance for potassium-ion battery. *Rare Met.* **2022**, *41* (7), 2259−2267.

(4) Zhang, H.; Yang, Y.; Ren, D.; Wang, L.; He, X. Graphite as anode materials: Fundamental mechanism, recent progress and advances. *Energy Storage Mater.* **2021**, *36*, 147−170.

(5) Li, M.; Lu, J.; Chen, Z.; Amine, K. 30 years of lithium-ion batteries. *Adv. Mater.* **2018**, *30* (33), No. 1800561.

(6) Yu, Y.; Yang, Z.; Liu, Y.; Xie, J. Achieving SEI preformed graphite in flow cell to mitigate initial lithium loss. *Carbon* **2022**, *196*, 589−595.

(7) Shim, J.; Striebel, K. A. Electrochemical characterization of thermally oxidized natural graphite anodes in lithium-ion batteries. *J. Power Sources* **2007**, *164* (2), 862−867.

(8) Billaud, J.; Bouville, F.; Magrini, T.; Villevieille, C.; Studart, A. R. Magnetically aligned graphite electrodes for high-rate performance Li-ion batteries. *Nat. Energy* **2016**, *1* (8), No. 16097.

(9) McShane, E. J.; Colclasure, A. M.; Brown, D. E.; Konz, Z. M.; Smith, K.; McCloskey, B. D. Quantification of Inactive Lithium and Solid−Electrolyte Interphase Species on Graphite Electrodes after Fast Charging. *ACS Energy Lett.* **2020**, *5* (6), 2045−2051.

(10) Kim, D. S.; Kim, Y. E.; Kim, H. Improved fast charging capability of graphite anodes via amorphous Al2O3 coating for high power lithium ion batteries. *J. Power Sources* **2019**, *422*, 18−24.

(11) Kim, N.; Chae, S.; Ma, J.; Ko, M.; Cho, J. Fast-charging high-energy lithium-ion batteries via implantation of amorphous silicon

nanolayer in edge-plane activated graphite anodes. *Nat. Commun.* **2017**, *8* (1), No. 812.
(12) Shi, J.; Ehteshami, N.; Ma, J.; Zhang, H.; Liu, H.; Zhang, X.; Li, J.; Paillard, E. Improving the graphite/electrolyte interface in lithium-ion battery for fast charging and low temperature operation: Fluorosulfonyl isocyanate as electrolyte additive. *J. Power Sources* **2019**, *429*, 67−74.
(13) Song, G.; Yi, Z.; Su, F.; Xie, L.; Wang, Z.; Wei, X.-X.; Xu, G.; Chen, C.-M. Boosting the Low-Temperature Performance for Li-Ion Batteries in LiPF6-Based Local High-Concentration Electrolyte. *ACS Energy Lett.* **2023**, *8* (3), 1336−1343.
(14) Yang, Y.; Fang, Z.; Yin, Y.; Cao, Y.; Wang, Y.; Dong, X.; Xia, Y. Synergy of Weakly-Solvated Electrolyte and Optimized Interphase Enables Graphite Anode Charge at Low Temperature. *Angew. Chem.* **2022**, *134* (36), No. e202208345.
(15) Zhang, S.; Xu, K.; Jow, T. Low temperature performance of graphite electrode in Li-ion cells. *Electrochim. Acta* **2002**, *48* (3), 241−246.
(16) Zhang, S.; Xu, K.; Jow, T. A new approach toward improved low temperature performance of Li-ion battery. *Electrochem. Commun.* **2002**, *4* (11), 928−932.
(17) Zhang, S.; Xu, K.; Jow, T. The low temperature performance of Li-ion batteries. *J. Power Sources* **2003**, *115* (1), 137−140.
(18) Abe, T.; Ohtsuka, M.; Sagane, F.; Iriyama, Y.; Ogumi, Z. Lithium ion transfer at the interface between lithium-ion-conductive solid crystalline electrolyte and polymer electrolyte. *J. Electrochem. Soc.* **2004**, *151* (11), A1950.
(19) Rodrigo, N. D.; Tan, S.; Shadike, Z.; Hu, E.; Yang, X.-Q.; Lucht, B. L. Improved low temperature performance of graphite/li cells using isoxazole as a novel cosolvent in electrolytes. *J. Electrochem. Soc.* **2021**, *168* (7), No. 070527.
(20) Song, G.; Yi, Z.; Su, F.; Xie, L.; Chen, C. New insights into the mechanism of LiDFBOP for improving the low-temperature performance via the rational design of an interphase on a graphite anode. *ACS Appl. Mater. Interfaces* **2021**, *13* (33), 40042−40052.
(21) Jiang, L. L.; Yan, C.; Yao, Y. X.; Cai, W.; Huang, J. Q.; Zhang, Q. Inhibiting Solvent Co-Intercalation in a Graphite Anode by a Localized High-Concentration Electrolyte in Fast-Charging Batteries. *Angew. Chem.* **2021**, *133* (7), 3444−3448.
(22) Rodrigo, N. D.; Jayawardana, C.; Rynearson, L.; Hu, E.; Yang, X.-Q.; Lucht, B. L. Use of Ethylene Carbonate Free Ester Solvent Systems with Alternative Lithium Salts for Improved Low-Temperature Performance in NCM622|| Graphite Li-ion Batteries. *J. Electrochem. Soc.* **2022**, *169* (11), No. 110504.
(23) Peled, E.; Menkin, S. SEI: past, present and future. *J. Electrochem. Soc.* **2017**, *164* (7), A1703−A1719.
(24) An, S. J.; Li, J.; Daniel, C.; Mohanty, D.; Nagpure, S.; Wood, D. L. The state of understanding of the lithium-ion-battery graphite solid electrolyte interphase (SEI) and its relationship to formation cycling. *Carbon* **2016**, *105*, 52−76.
(25) Nan, B.; Chen, L.; Rodrigo, N. D.; Borodin, O.; Piao, N.; Xia, J.; Pollard, T.; Hou, S.; Zhang, J.; Ji, X.; et al. Enhancing Li+ transport in NMC811|| graphite lithium-ion batteries at low temperatures by using low-polarity-solvent electrolytes. *Angew. Chem., Int. Ed.* **2022**, *61* (35), No. e202205967.
(26) Cheng, Q.; Yuge, R.; Nakahara, K.; Tamura, N.; Miyamoto, S. KOH etched graphite for fast chargeable lithium-ion batteries. *J. Power Sources* **2015**, *284*, 258−263.
(27) Cai, W.; Yan, C.; Yao, Y.-X.; Xu, L.; Xu, R.; Jiang, L.-L.; Huang, J.-Q.; Zhang, Q. Rapid Lithium Diffusion in Order@ Disorder Pathways for Fast-Charging Graphite Anodes. *Small Struct.* **2020**, *1* (1), No. 2000010.
(28) Yuge, R.; Tamura, N.; Manako, T.; Nakano, K.; Nakahara, K. High-rate charge/discharge properties of Li-ion battery using carbon-coated composites of graphites, vapor grown carbon fibers, and carbon nanohorns. *J. Power Sources* **2014**, *266*, 471−474.
(29) Gao, Y.; Rojas, T.; Wang, K.; Liu, S.; Wang, D.; Chen, T.; Wang, H.; Ngo, A. T.; Wang, D. Low-temperature and high-rate-charging lithium metal batteries enabled by an electrochemically active monolayer-regulated interface. *Nat. Energy* **2020**, *5*, 534−542.
(30) Urchaga, P.; Weissmann, M.; Baranton, Sv.; Girardeau, T.; Coutanceau, C. Improvement of the Platinum Nanoparticles−Carbon Substrate Interaction by Insertion of a Thiophenol Molecular Bridge. *Langmuir* **2009**, *25* (11), 6543−6550.
(31) Nickol, A.; Heubner, C.; Schneider, M.; Michaelis, A. Understanding Low Temperature Limitations of LiNi0. 5Co0. 2Mn0. 3O2 Cathodes for Li-Ion Batteries. *J. Electrochem. Soc.* **2022**, *169* (5), No. 050511.
(32) Xu, F.; Wang, M.-x.; Sun, L.; Liu, Q.; Sun, H.-f.; Stach, E. A.; Xie, J. Enhanced Pt/C catalyst stability using p-benzensulfonic acid functionalized carbon blacks as catalyst supports. *Electrochim. Acta* **2013**, *94*, 172−181.
(33) Liu, Y.; Liu, Q.; Xin, L.; Liu, Y.; Yang, F.; Stach, E. A.; Xie, J. Making Li-metal electrodes rechargeable by controlling the dendrite growth direction. *Nat. Energy* **2017**, *2*, No. 17083.
(34) Pan, Q.; Wang, H.; Jiang, Y. Covalent modification of natural graphite with lithium benzoate multilayers via diazonium chemistry and their application in lithium ion batteries. *Electrochem. Commun.* **2007**, *9* (4), 754−760.
(35) Baranton, S.; Bélanger, D. In situ generation of diazonium cations in organic electrolyte for electrochemical modification of electrode surface. *Electrochim. Acta* **2008**, *53* (23), 6961−6967.
(36) Verma, P.; Novák, P. Formation of artificial solid electrolyte interphase by grafting for improving Li-ion intercalation and preventing exfoliation of graphite. *Carbon* **2012**, *50* (7), 2599−2614.
(37) Bauer, M.; Pfeifer, K.; Luo, X.; Radinger, H.; Ehrenberg, H.; Scheiba, F. Functionalization of Graphite Electrodes with Aryl Diazonium Salts for Lithium-Ion Batteries. *ChemElectroChem* **2022**, *9* (8), No. e202101434.
(38) Markey, B.; Zhang, M.; Robb, I.; Xu, P.; Gao, H.; Zhang, D.; Holoubek, J.; Xia, D.; Zhao, Y.; Guo, J.; et al. Effective upcycling of graphite anode: healing and doping enabled direct regeneration. *J. Electrochem. Soc.* **2020**, *167* (16), No. 160511.
(39) Rjeb, A.; Letarte, S.; Tajounte, L.; El Idrissi, M. C.; Adnot, A.; Roy, D.; Claire, Y.; Kaloustian, J. Polypropylene natural aging studied by X-ray photoelectron spectroscopy. *J. Electron Spectrosc. Relat. Phenom.* **2000**, *107* (3), 221−230.
(40) Jung, Y.; Kang, B. Understanding abnormal potential behaviors at the 1st charge in Li 2 S cathode material for rechargeable Li−S batteries. *Phys. Chem. Chem. Phys.* **2016**, *18* (31), 21500−21507.
(41) Cai, W.; Yao, Y.-X.; Zhu, G.-L.; Yan, C.; Jiang, L.-L.; He, C.; Huang, J.-Q.; Zhang, Q. A review on energy chemistry of fast-charging anodes. *Chem. Soc. Rev.* **2020**, *49*, 3806−3833.
(42) Shen, Y.; Shen, X.; Yang, M.; Qian, J.; Cao, Y.; Yang, H.; Luo, Y.; Ai, X. Achieving Desirable Initial Coulombic Efficiencies and Full Capacity Utilization of Li-Ion Batteries by Chemical Prelithiation of Graphite Anode. *Adv. Funct. Mater.* **2021**, *31*, No. 2101181.
(43) Dong, W.; Wang, W.; Shen, D.; Sun, W.; Zhao, M.; Meng, L.; Yang, S.; Zhu, X.; Chi, H.; Dong, L. Structure and Low-temperature Performance of Waste Graphite Used in Lithium-ion Battery Anode. *ChemistrySelect* **2022**, *7* (8), No. e202104547.
(44) Günter, F. J.; Habedank, J. B.; Schreiner, D.; Neuwirth, T.; Gilles, R.; Reinhart, G. Introduction to electrochemical impedance spectroscopy as a measurement method for the wetting degree of lithium-ion cells. *J. Electrochem. Soc.* **2018**, *165* (14), A3249.
(45) Jow, T. R.; Delp, S. A.; Allen, J. L.; Jones, J.-P.; Smart, M. C. Factors limiting Li+ charge transfer kinetics in Li-ion batteries. *J. Electrochem. Soc.* **2018**, *165* (2), A361.
(46) Abe, T.; Fukuda, H.; Iriyama, Y.; Ogumi, Z. Solvated Li-ion transfer at interface between graphite and electrolyte. *J. Electrochem. Soc.* **2004**, *151* (8), A1120.
(47) Xu, K. Charge-transfer" process at graphite/electrolyte interface and the solvation sheath structure of Li+ in nonaqueous electrolytes. *J. Electrochem. Soc.* **2007**, *154* (3), A162.

https://doi.org/10.1021/acsaem.3c02203
ACS Appl. Energy Mater. 2023, 6, 12371−12378